Identification of novel potential antiviral inhibitors of the main protease enzyme of the feline infectious peritonitis virus using artificial intelligence and molecular docking tools (#106669)

First submission

Guidance from your Editor

Please submit by **10 May 2025** for the benefit of the authors (and your token reward) .

Structure and Criteria
Please read the 'Structure and Criteria' page for guidance.

Author notes
Have you read the author notes on the guidance page?

Raw data check
Review the raw data.

Image check
Check that figures and images have not been inappropriately manipulated.

If this article is published your review will be made public. You can choose whether to sign your review. If uploading a PDF please remove any identifiable information (if you want to remain anonymous).

Files
Download and review all files from the materials page.

8 Figure file(s)
3 Table file(s)
1 Other file(s)

Structure and Criteria

Structure your review

The review form is divided into 5 sections. Please consider these when composing your review:

1. **BASIC REPORTING**
2. **EXPERIMENTAL DESIGN**
3. **VALIDITY OF THE FINDINGS**
4. General comments
5. Confidential notes to the editor

You can also annotate this PDF and upload it as part of your review

When ready submit online.

Editorial Criteria

Use these criteria points to structure your review. The full detailed editorial criteria is on your guidance page.

BASIC REPORTING

- Clear, unambiguous, professional English language used throughout.
- Intro & background to show context. Literature well referenced & relevant.
- Structure conforms to PeerJ standards, discipline norm, or improved for clarity.
- Figures are relevant, high quality, well labelled & described.
- Raw data supplied (see PeerJ policy).

EXPERIMENTAL DESIGN

- Original primary research within Scope of the journal.
- Research question well defined, relevant & meaningful. It is stated how the research fills an identified knowledge gap.
- Rigorous investigation performed to a high technical & ethical standard.
- Methods described with sufficient detail & information to replicate.

VALIDITY OF THE FINDINGS

- **Impact and novelty is not assessed.** Meaningful replication encouraged where rationale & benefit to literature is clearly stated.
- All underlying data have been provided; they are robust, statistically sound, & controlled.
- Conclusions are well stated, linked to original research question & limited to supporting results.

Standout reviewing tips

The best reviewers use these techniques

Tip	*Example*
Support criticisms with evidence from the text or from other sources	*Smith et al (J of Methodology, 2005, V3, pp 123) have shown that the analysis you use in Lines 241-250 is not the most appropriate for this situation. Please explain why you used this method.*
Give specific suggestions on how to improve the manuscript	*Your introduction needs more detail. I suggest that you improve the description at lines 57- 86 to provide more justification for your study (specifically, you should expand upon the knowledge gap being filled).*
Comment on language and grammar issues	*The English language should be improved to ensure that an international audience can clearly understand your text. Some examples where the language could be improved include lines 23, 77, 121, 128 – the current phrasing makes comprehension difficult. I suggest you have a colleague who is proficient in English and familiar with the subject matter review your manuscript, or contact a professional editing service.*
Organize by importance of the issues, and number your points	*1. Your most important issue* *2. The next most important item* *3. …* *4. The least important points*
Please provide constructive criticism, and avoid personal opinions	*I thank you for providing the raw data, however your supplemental files need more descriptive metadata identifiers to be useful to future readers. Although your results are compelling, the data analysis should be improved in the following ways: AA, BB, CC*
Comment on strengths (as well as weaknesses) of the manuscript	*I commend the authors for their extensive data set, compiled over many years of detailed fieldwork. In addition, the manuscript is clearly written in professional, unambiguous language. If there is a weakness, it is in the statistical analysis (as I have noted above) which should be improved upon before Acceptance.*

Identification of some novel potential antiviral inhibitors of the main protease enzyme of the Feline infectious peritonitis virus using artificial intelligence and molecular docking tools

Mohd Yasir Khan [1], **Abid Ullah Shah** [2], **Nithyadevi Duraisamy** [1], **Nadine G Mowaed** [3], **Reda Nacif El Alaoui** [1], **Mohammed Cherkaoui** [1], **Maged Gomaa Hemida** [Corresp. 2]

[1] Department of Computer Science, College of Digital Engineering and Artificial Intelligence, Long Island University, Brooklyn, NY, United States

[2] Department of Veterinary Biomedical Sciences, College of Veterinary Medicine, Long Island University, Brookville, NY, United States

[3] Veterinary Biomedical Sciences, Long Island University, Brookville, NY, United States

Corresponding Author: Maged Gomaa Hemida
Email address: maged.hemida@liu.edu

Background. Feline infectious peritonitis virus (FIPV) is one of cats' most serious viral infections. The FIPV infection induces a complicated syndrome in the affected cats, including immunosuppression and severe inflammatory conditions. Unfortunately, these vaccines cannot prevent cats from getting infected with these viral infections. There is ongoing research on preparing antiviral therapies against FIPV in cats. However, these are still in clinical trials and have not been fully approved by the drug authorities in many countries, including the USA. Targeting the main viral proteases is one of the promising trends in the drug design of many viral diseases, including coronaviruses. The main goal of the current study was to repurpose and test the efficacy of some known antiviral drugs to treat FIPV infection in cats by targeting the FIPV-main protease enzyme. **Methods.** To achieve these goals, we used the in-silico prediction and molecular docking tools to screen and identify some drugs targeting FIPV-MPro. We used the docking and binding energies as the main parameters for selecting target compounds (FIPV-MPro). **Results.** Our results show that out of the 15 antiviral and immunomodulatory compounds, the top-ranked inhibitors for the FIPV-Mpro are (Michael acceptor inhibitors (N3), Sofosbuvir, and methotrexate). In conclusion, our results confirmed the potential applications of the predicted FIPV-Mpro inhibitors either independently or in combination with other immune-modulatory compounds. Further in vitro and in vivo studies are encouraged to test the efficacy of these identified compounds as potent inhibitors for the MPro of the FIPV in cats. This study will pave the way for the development of novel drugs that treat FIPV infection in cats.

Identification of potential inhibitors of the main protease enzyme of the Feline infectious peritonitis virus using molecular docking and dynamic simulation

Mohd Yasir Khan[1], Abid Ullah Shah[2], Nithyadevi Duraisamy[1], Nadine Moawad[2], Reda Nacif El-Alaoui[1], Mohammed Cherkaoui[1], Maged Gomaa Hemida[2]*

[1] Department of Computer Science, College of Digital Engineering and Artificial Intelligence, Long Island University, Brooklyn, New York, USA

[2] Department of Veterinary Biomedical Sciences, College of Veterinary Medicine, Long Island University, Brookville, New York, USA

***Corresponding Author:**
Maged Hemida[2]
720 Northern Boulevard, Brookville, New York, 11548, USA
Email: maged.hemida@liu.edu

Abstract

Background.

Feline infectious peritonitis virus (FIPV) is one of cats' most serious viral infections. The FIPV infection induces a complicated syndrome in the affected cats, including immunosuppression and severe inflammatory conditions. Unfortunately, these vaccines cannot prevent cats from getting infected with these viral infections. There is ongoing research on preparing antiviral therapies against FIPV in cats. However, these are still in clinical trials and have not been fully approved by the drug authorities in many countries, including the USA. Targeting the main viral proteases is one of the promising trends in the drug design of many viral diseases, including coronaviruses. The main goal of the current study was to repurpose and test the efficacy of some known antiviral drugs to treat FIPV infection in cats by targeting the FIPV-main protease enzyme.

Methods.

We used the in-silico prediction and molecular docking tools to screen and identify some drugs targeting FIPV-MPro to achieve these goals. The research method was started by building a screening pharmacokinetic associated variables of the compound, then used to design a new potential inhibitor by employing the docking and molecular dynamic simulation to evaluate the

interaction of all complexes using the Standard dynamics cascade protocol of Biovia Discovery studio.

Results.

Our results show that out of the 15 antiviral and immunomodulatory compounds, the top-ranked inhibitors for the FIPV-Mpro are reference standard inhibitor (N3), Sofosbuvir, and the GS-441524 out of which GS-441524 was suggested as Mpro-inhibitor on the basis of further investigation through molecular dynamics simulation method. In conclusion, our results confirmed the potential applications of the predicted FIPV-Mpro inhibitors either independently or in combination with other immune-modulatory compounds. Further *in vitro* and *in vivo* studies are encouraged to test the efficacy of these identified compounds as potent inhibitors for the Mpro of the FIPV in cats. This study will pave the way for the development of novel drugs that treat FIPV infection in cats.

1. Introduction

FIPV belongs to the order Mononegavirales, family coronaviruses and genus alphacoronavirus, species alphacoronavirus-1 and subspecies feline coronavirus (FCoV). The viral genome is a single molecule of a positive-sense RNA. The FIPV genome has a typical coronavirus genome organization and encodes 11 proteins, including four structural and seven non-structural proteins. The major non-structural proteins encoded by Gene-1 (ORF1a and ORF1b with ribosomal frameshifting in between) reside at the 5' two-thirds of the genome. Other non-structural proteins of the FCoV are encoded by the 3 abc and 7a/b genes. The structural proteins are Spike (s), Envelope (E) Membrane (M), and the nucleocapsid (N). The ORF1a/b is further processed by some viral encoded proteases into 16 non-structural proteins (NSP-1-NSP16) *(Brierley, Digard, & Inglis, 1989)*. The FIPV-3c protein is important for virus replication and contributes to viral virulence and tissue tropism *(Jaimes & Whittaker, 2018)*. Although the function of the FIPV-7ab proteins is not fully understood, they might play important roles in viral immune evasion, particularly as an antagonist for the IFN-type I *(Dedeurwaerder et al., 2013)*.

Based on the FIPV-S sequences, the virus is classified into two serotypes. Serotype-I is designated as FIPV, which is the most virulent serotype and causes a lethal infection in cats

(Hohdatsu, Okada & Koyama, 1991). Although FIPV infection in cats is not contagious (it does not spread easily among cat populations), until now, the prognosis of cats infected with the virus has always been fatal in most cases *(Kennedy, 2020)*. The absence of vaccines that could protect cats against FIPV infection makes antiviral therapy the only remedy to treat cats from FIPV infection. Several antiviral compounds, particularly nucleoside analogs and interferons, have been tried to inhibit or interrupt the FIPV replication cycle at various stages *(Murphy et al., 2018; Pedersen et al., 2019; Addie et al., 2020; Dickinson et al., 2020)*. This approach includes the application of a single or a combination of different compounds together to ensure the robust inhibition of viral replication *(Schmied et al., 2024)*. Coronaviruses' main protease (Mpro) is one of the most important targets for the design of antiviral therapy for several coronaviruses, including the Middle East Respiratory Syndrome coronavirus (MERS-CoV), the Severe Acute Respiratory Syndrome virus-2 (SARS-CoV-2), the porcine epidemic diarrhea virus (PEDV)
as well as the FIPV *(Wang et al., 2020)*.

The main reason for targeting CoVs-Mpro is their essential role in polyprotein processing during viral replication. In the current study we used the in-silico drug design tools to predict the efficacy of 15 selected antiviral, anti-inflammatory, and immune-modulatory compounds on the inhibition of the FIPV-Mpro enzyme (standard inhibitor-N3) compound and nucleoside precursors/analog such as Oxipurinol, Favipiravir, Pentoxifylline, Baricitinib, Methotrexate, Gemcitabine, Galidesivir, Ribavirin, 6-Azauridine, GS441524, Mizoribine, Sofosbuvir, Molnupiravir, and Tenofovir. We used the crystal structure of the FIPV-Mpro available in the public domain and analyzed the binding sites of each compound to these in the FIPV-Mpro. This approach will provide more insights into the inhibitory actions of the selected compounds on the FIPV-Mpro. These potential FIPV drugs could be used independently or in combination to inhibit FIPV replication, suppress the severe inflammatory conditions associated with viral infections, and enhance the immune response against the viral infection. It will also pave the way for more research to do more functional characterization of the potential inhibitory effects of these compounds on the FIPV replication in the in vitro and in vivo models. This approach will lead to the production of effective antiviral therapy against FIPV infection in cats.

2. Materials and Methods

2.1 Receptor protein and ligand file retrieval

The Feline infectious peritonitis virus (FIPV) main protease (FIPV-Mpro) protein in complex with ligand N-(5-methylisoxazol-3-yl)-3-tosyl propanamide (N3) and its 3D structure was downloaded from the RCSB-Protein Data Bank (PDB) https://www.rcsb.org/, in the PDB file *(Ali et al., 2017)*. The protein data bank is a library for biological compounds that stores three-dimensional structural information. The PDB ID of FIPV N3-Mpro complex is 5EU8. Further, all nucleoside precursors and analogs as ligands are retrieved from the PubChem database https://pubchem.ncbi.nlm.nih.gov. The PubChem compound ID (CID) for each ligand is given (Table 1).

2.2 ADMET and drug-likeness analysis of selected ligands

The selected nucleoside precursors and analogs were screened for detailed analysis of physicochemical descriptors, drug-likeness through the Lipinski rule of five, and pharmacokinetics-associated variables, i.e., absorption, distribution, metabolism, and excretion and toxicity (ADMET) *(Bultum et al., 2022)*.

In order to assist in the early identification of potential mutagenic, *in silico* prediction of compound mutagenicity, the Ames test is the most widely used assay for testing the mutagenicity-assisted toxicity of a compound *(Chu et al., 2021)*. The AMES toxicity prediction and ADMET Properties were analyzed by using AMES Test and ADMET protocol of Biovia Discovery Studio v24.1.0.321712.

2.3 Docking of compounds with the Mpro

The molecular docking approach can be used to model the interaction between a Mpro protein with nucleoside precursors and nucleoside analogs. The interactions between these small molecules and proteins at the atomic level, molecular docking, help us understand how these molecules bind and function within biological processes *(Meng et al., 2011; Agu et al., 2023)*. In the CDOCKER tool from Biovia Discovery Studio docking protocol, we typically use 10 docking poses for ligand. For each dock ligand pose, the higher positive values of CDOCKER interaction energy score and calculated binding energy (ΔG) indicate more favorable binding *(Gagnon, Law & Brook, 2016; Ding et al., 2020; Agu et al., 2023)*.

These computational tools enable the visualization of the ligand-target interaction (molecular docking) and the identification of the compounds that bind more efficiently with the target *(Agu et al., 2023)*. This analysis typically involves examining the docking scores, ligand-protein interactions, and the visualization of the docked complexes. To describe the defining binding site in

protein, interaction binding affinity score (-CDOCKER interaction score), calculation of binding energy (ΔG), is likely an internal step within Biovia Discovery Studio v24.1.0.321712.

2.4 MM-GBSA calculations- Molecular mechanics-generalized born surface area

The binding free energy of the observed protein-ligand complexes was measured using the MM-GBSA approach, which integrates molecular mechanics (MM) force fields with a generalized Born and surface area continuum with a non-implicit solvation model. The MM-GBSA calculation incorporates the CHARMm force field, with partial charge estimation using Memory Rone. The Di-electric constant is 1, and the minimum non-bond higher and lower cutoff distance is 12 and 10 Å. The MM-GBSA was determined in this study using the equation ΔG = E_complex (minimized)– [E_ligand (minimized) + E_receptor (minimized)] from Biovia Discovery Studio v24.1.0.321712. The default setting employed to compute MM-GBSA involved rendering all protein atoms rigid while the ligand atoms are relaxed.

2.5 Molecular dynamics (MD) simulation

Based on in vitro analysis, docking energies, and conformational pose analysis, four best complexes were selected for MD simulation *(Arnittali et al., 2019; Ahmad et al., 2021)*. To further explore the dynamic behavior of ligand–protein complexes, the best-predicted top hits of compounds and N3 (reference standard) with respect to Mpro-protein were selected to perform 50,000 picoseconds (ps) through standard dynamics cascade simulation. To generate the molecular topology files for protein complex and to create the topology of ligands, used CHARMm36 force field. The simulation system consists of an explicit boundary solvent model, an orthorhombic box with a minimal distance of 7 nm between the protein surface and the edge of the box, neutralized with the inclusion of cation-type sodium (Na) and anion-type Chloride (Cl) counter-ions. For the energy minimization, the steepest descent (minimization 1) with RMS gradient one and conjugate gradient (minimization 2) with RMS gradient 0.1. Both minimization algorithms were used for 50,00 steps. The heating phase was performed using simulation time 4 ps with time step 2 fs. For immersion, the initial temperature is 50 and the target temperature 300 K with a save results interval of two ps.

The equilibration phases were carried out for a 200 ps (picosecond) simulation run with a 2 fs (femtosecond) time step, and the saved result interval is two ps. The particle-mesh-Ewald (PME) algorithm was used for long-range electrostatic interactions with fourth-order cubic interpolation and

kappa 0.34 Å grid spacing. The advanced dynamic integrator used the Leapfrog Verlet algorithm with applied shake constraint. The implicit solvent model was used with dielectric constant 1, Nonbond list radius cutoff 14 in which nonbond higher cutoff distance is 12 and nonbond lower cutoff distance is 10. The production step of a standard dynamic cascade of MD simulation was carried out for 50 ns (50000 picoseconds). Trajectory analysis was done to confirm hydrogen bond distance, Root Mean Square Deviation (RMSD), Root Mean Square Fluctuation (RMSF), and Radius of Gyration (RG) of each system. The stability of the complex is indicated by the highest potential inhibitor from the stable complex protein-ligand through Biovia Discovery Studio v24.1.0.321712.

3. Results:

3.1 Pharmacological potential of nucleoside precursors and analogs

For drug screening, Lipinski's Rule of five includes criteria such as molecular weight (M.W. ≤ 500 Da), hydrogen bond donors (HBD ≤ 5), hydrogen bond acceptors (HBA ≤ 10), and the octanol-water partition coefficient (LogP ≤ 5) *(Ahmad et al., 2024)*. Our drug-likeness analysis portrayed that selected nucleoside analogs fall under the acceptable scores of Lipinski's **rule** of five with a few exceptions. Particularly, the chemical structure of methotrexate showed 7 HBD and 13 HBA violated 2 rules of Lipinski's, whereas compound sofosbuvir also violated 2 rules of Lipinski's exhibited 12 HBA and M.W. 529, which we overruled for further screening. In contrast, the N3 (reference standard) exhibited 14 HBA, 6 HBD, and M.W. 680.79 Da, violating the rules of Lipinski (Table 1). The ALogP analysis revealed that all the nucleoside analogs with the standard N3 have LogP values below 5, which is within the desirable threshold (LogP ≤ 5). Any compound has a molecular polar surface area (MPSA) ≥140 Å², and struggle to cross cell membranes effectively, which could result in poor absorption and bioavailability, especially when taken orally. Any compounds has an MPSA value between 75-140 Å² are typically considered to have good permeability properties, while compounds with values higher than 140 Å² are more likely to face issues with membrane permeability and absorption *(Veber et al., 2002)*. In our study, all the compounds exhibited the range of MPSA below the desired threshold (140 Å²) except Standard reference N3, Methotrexate, and Sofosbuvir (Table 1).

3.2 ADMET variables and AMES test analysis of Nucleoside analogs and precursors

The parameter ADMET solubility is defined by the base 10 logarithm of the molar solubility in water (Log-SW), as predicted by the regression (Table S1). On the basis of Log (SW), we defined the solubility of compounds by categorical solubility level. The solubility analysis revealed that selected nucleoside analogs exhibited better aqueous solubility, ranging solubility level from 2-4 (Table 2), which shows its drug likeliness solubility level (Level 0: extremely low, 1: No-very low but possible, 2: Yes-but low, 3: Yes-good, 4: Yes-optimal, 5: No-too soluble). The good solubility compounds could be explained by the higher number of HBs formed by the nucleoside analogs in aqueous solutions (Table 2 and Table S1). In the ADMET method of Biovia discovery studio, the blood-brain barrier (BBB) model contains a quantitative linear regression model for the prediction of blood-brain penetration, as well as 95% and 99% confidence ellipses in the ADMET_PSA_2D, ADMET_AlogP98 plane. The model was derived from over 800 compounds that are known to enter the CNS after oral administration (Egan et al., 2002). The model includes four prediction levels within the 95% and 99% confidence ellipsoids: level 0 (Very high penetrant), 1 (High), 2 (Medium), 3 (Low) and 4 (Undefined- No prediction is made for compounds outside the 95% and 99% confidence ellipsoids). BBB penetration level for the selected compounds ranged from 3 to 4, indicating either low or very low penetration and absorption across the blood-brain barrier (Table 2). Additionally, the estimation of the level of plasma protein binding (PPB) plays a crucial role in the distribution of a drug from circulation to the target organs. The plasma protein binding model predicts whether a compound is likely to be highly bound (>= 90% bound) to carrier proteins in the blood. The negative values (ranging from -4.1131 to -38.845) indicate that these compounds do not have strong PPB (Table S1). These values likely reflect the binding affinity of the compounds to plasma proteins like albumin. More negative values typically suggest weaker binding or less affinity for plasma proteins. A low or weak binding indicates that a greater proportion of the drug will be available in its free (active) form in circulation.

The key to intestinal absorption (IA), ADMET absorption level, is determined by the Mahalanobis distance (ADMET_Absorption_T2_2D) of the compound in the ADMET_PSA_2D and ADMET_AlogP98 plane. This distance is compared to the center of the region of chemical space defined by well-absorbed compounds. Based on this distance, the compound is categorized into one of four absorption levels (good:0, moderate:1, low:2, very low or poor:3). Therefore, the efficiency of drug relies on their intestinal absorption (IA) to the distribution to target organs where the absorption range are considered low, middle and high, respectively *(Ahmad et al., 2021)*. The

predicted absorption levels from the ADMET model of all the compounds ranged from 0 to 3 (Table 2). Compounds with absorption levels of 0-1 are predicted to have good to moderate absorption, suggesting enhanced bioavailability, which may be linked to the potent pharmacological actions of these nucleoside precursors and analogs. In contrast, the reference Mpro-standard inhibitor (N3) and inhibitors such as methotrexate, sofosbuvir, Mizoribine, Ribavirin, and 6-Azauridine were predicted to have an absorption level of 3, suggesting poor intestinal absorption for these inhibitors. In ADMET, CYP2D Prediction indicates the predicted classification, using a cutoff Bayesian score of 0.161 to minimize false positives and false negatives and the Bayesian score calculated by a model, used to classify a compound as either a CYP2D6 inhibitor or non-inhibitor *(Santos et al., 2017; Kato H, 2020)*. The CYP2D6 values for all the compounds are predominantly negative, ranging from -0.67 to -12.21 (Table S1). According to the ADMET CYP2D6 model, more negative values indicate weaker binding or less interaction with the enzyme. The model's false predictions suggest that these compounds are not significant inhibitors or binders of the CYP2D6 enzyme (Table 2).

The hepatotoxicity prediction values represent the prediction scores or risk scores for hepatotoxicity. Typically, a score indicates the likelihood of hepatotoxicity, with negative scores often associated with a lower risk and positive scores associated with a higher risk (Table S1). The ADMET hepatotoxicity prediction values reflect the model's output, where compounds with higher positive values (3.3959 and 23.9597) are more likely to be predicted as hepatotoxic (True), and those with negative values such as Standard inhibitor N3 and Pentoxifylline (-7.21011, -12.2658) are less likely to be hepatotoxic (False) (Table 2 and S1). On the other hand, the test for prediction (TOPTAK prediction methods) of mutagen detection is based on the Ames prediction. The Ames test values are mostly negative (Table S1), which indicates that these compounds are unlikely to cause mutations and do not pose a significant genetic risk in terms of mutagenicity. Any compound that has positive or near-zero Ames values tends to be classified as mutagenic (Table 2).

3.3 Mpro-Ligands Interaction and Binding Energy

MPro in complex with N3 compound in X-ray crystal structure from RCSB PDB database (PDB ID:5eu8; 1.80 Å resolution) was chosen as the receptor for different ligand docking. The PubChem CID for all nucleoside analogs as ligands (Table 1). In this attempt to filter suitable and compounds

have the best binding to FIPV-Mpro, our molecular docking studies revealed a strong interaction of nearly all the selected compounds with binding energies (ΔG) from -7.4 to -4.8 kcal/mol and CDOCKER interaction energy score for binding affinities from 68 to 14 against the active pocket of FIPV-Mpro (Table 3). Among nucleoside precursors and analogs, nucleoside analog Sofosbuvir topped the binding energy and affinity score (ΔG: -7.38 kcal/mol and CDOCKER interaction energy score: 39.34) and interacted with His41, Cys144, Leu164, Glu165, Leu166, and Pro188 residues of FIPV-Mpro active pocket (Fig. 1 and table 3). Whereas, the interaction of another top-scoring nucleoside analog, i.e., GS-441524 with FIPV- Mpro was favored by ΔG of -7.2 kcal/mol, whereas binding affinity score (CDOCKER interaction energy score: 43) and interacting residues of the Mpro with GS-441524 is given in table 3. The interaction pattern of the top two ligands, sofosbuvir, GS-441524, and standard N3 is also shown in (Fig. S1-3-2D). The other top-scoring nucleoside precursors and analogs, except sofosbuvir and GS-441524, are Methotrexate, Pentoxifylline, and Molnupiravir, exhibits binding with some common residues of the active pocket of FIPV-Mpro i.e., Val26, His41, Thr47, Ala141, Cys144, His162, His163, Leu164, Glu165, Pro188 and Ser189 (Table 3 and Fig. S4-6). In contrast, the best docking pose of the standard inhibitor (N3) exhibited a binding affinity to Mpro with low binding energy (ΔG= -7.11 Kcal/mol) (Table 3). However, the highest -CDOCKER energy and -CDOCKER interaction energy score (positive value) referred to the most favorable binding of ligand to the protein. The -CDOCKER energy and -CDOCKER interaction energy scores for the N3 best docking pose are 88.72 and 68.11 (Table 3). The interaction between the Mpro and the N3 compound involves some key amino acid residues and bonds, including (Asn25, His41, Ala141, Cys144 Leu164, Glu165, Leu166, Gly167, Pro188, and Met190) **as** shown in (Figs. 1, 2D and Table 3).

3.4 Ligand-Protein MM-GBSA calculations-Pre- Pre MD-simulation

The calculation of MM-GBSA for all the compounds was carried out for the top 10 hits and the standard (N3). The top hit of sofosbuvir and GS-441524 displayed the highest free energy (−106.82 kcal/mol and -91.02 kcal/mol), predicting the stability of its complex with the Mpro and validating the docking results. These top hits from sofosbuvir are considered as Ligand 1 and GS-441524 as Ligand-2, compared with the standard N3 compound (Table-3). The remaining hits displayed comparable free energy when compared to the standard (−90.64 kcal/mol), with only compound Oxipurinol exhibiting a significantly lowered free energy of −35.16 kcal/mol (Table 3).

3.5 Molecular dynamics simulation

Proteins play a crucial role in various structural and functional processes, including microbial pathogenesis, by mediating receptor-based internalization and replication. Therefore, investigating how ligands such as nucleoside analogs affect the structural stability of FIPV-Mpro is essential to understanding their potential to block viral internalization and replication. Molecular dynamics simulation (MD simulation) is valuable for examining protein structures in silico. In this study, we selected the top-performing nucleoside analogs with the lowest ΔG values from CDOCKER-docking studies such as Sofosbuvir (Ligand 1), GS-441524 (Ligand 2), and N3 (standard inhibitor) for FIPV-Mpro, for 50,000 picoseconds (ps) MD simulations. A comprehensive analysis of trajectories, including RMSD, RMSF, RG, the number of hydrogen bonds established, and hydrogen bond distance, was measured to explore the stability and molecular interactions of the protein-ligand complexes compared to a standard inhibitor (N3).

3.5.1 RMSD calculations conferring stability of ligand-protein complexes.

The RMSD value of <2 Å is considered desirable and indicates similarity to the standard N3-Mpro complex. A lower RMSD value also suggests greater stability of the protein-ligand complexes. In this study, the RMSD of the ligand-protein complexes were significantly less fluctuating for GS-441524 and Sofosbuvir as compared to N3 during the simulations, indicating high stability of GS-441524 and Sofosbuvir with Mpro (Fig. 2). The average RMSDs of the backbone atoms for the GS-441524-Mpro, Sofosbuvir -Mpro and N3-Mpro ranged between 1 and 3 nm. The average RMSDs of the backbone atoms for the GS-441524–Mpro complexes were 2.2 Å of two MD Runs, respectively. The complex of Ligand 2- GS-441524 showed stability after the initial 0-12000 ps, while it showed slight fluctuation after the 8000-11000 ps (Fig. 2) with the FIPV-Mpro during MD, which quickly stabilized again to the average RMSD (2.2 Å). The complex of Ligand 1-Sofosbuvir-Mpro showed stability after the initial 0-17000 ps, while it showed slight fluctuation after the 17000-21000 ps (Fig. 2) with the FIPV-Mpro during MD, which quickly stabilized again to the average RMSD (2.8 Å). Conversely, the standard compound- N3-Mpro complex also showed an average RMSD of 2.7 Å, MD runs, respectively.

3.5.2 analysis of the stability and mobility of complexes-RMSF

The predicted RMSF graphs of the C-α atom of all five complexes were plotted against the interacted residues based on the trajectory period of the MD simulation. All the residues in docking complexes

have fluctuated around 0.5-3 Å in the simulation time scale. The RMSF values for the amino acids in the Sofosbuvir-Mpro complex were notably lower than those in the N3-Mpro complexes, while the compound-Mpro complexes suggested near equal residue mobility Mpro protein with N3-inhibitor complex (Fig. 3). The significance of the low RMSF values from the RMSF analysis being an essential tool in the identification of the rigid and flexible sections of the protein structure. This conclusion is further validated after considering their low Radius of Gyration (RG) values, which indicated the low flexibility of both standard and inhibitor complexes.

3.5.3 Complex compactness analysis- Radius of gyration (RG)

The radius of Gyration (RG) is used to determine whether the complexes are stably folded or unfolded during the MD simulation. The average RG value of two MD Runs of N3-Mpro was calculated to be around 22.2 Å. Furthermore, the average RG values of Sofosbuvir (Ligand-1) with Mpro complex and GS-441524 (Ligand 2) with Mpro were 21.9 Å and respectively, significantly similar to reference N3-Mpro complex, which is 22.2 Å (Fig. 4). As a result, it can be observed, that GS-441524-Mpro and Sofosbuvir-Mpro complex exhibited relatively similar behavior of compactness and consistent values of RG as compared to the reference standard N3-Mpro. It indicates that these are perfectly superimposed with each other and have high stability.

3.5.4 Hydrogen bonds and their distance-Complex stability

Molecular dynamics simulation was carried out over a 50000 ps simulation time for all new compounds against Mpro protein. To investigate the stability of the ligand interaction with protein, the measurement of intermolecular hydrogen bond development and its distance between ligand-protein complexes were evaluated. The complexes of sofosbuvir (Ligand-1) and N3 (Standard) with Mpro protein protease maintained two hydrogen bonds throughout the entire simulation time. However, the GS-441524 (Ligand-2) was able to maintain three hydrogen bonds throughout the simulation time (Fig. 5 B and D). Furthermore, all three complexes in two runs of MD were able to maintain four hydrogen bonds through the majority of the conformations of the simulation (Fig. 5 A-F).

On the other hand, the estimation of the hydrogen bond distance monitored between the ligands and the interacted residues of the Mpro-protein, the sofosbuvir (Ligand 1), showed four hydrogen bonding interactions during simulation time with Mpro protein. In the depicted hydrogen

bond distance graph of two MD simulation runs for sofosbuvir, residue Cys144, Gly167, THR, and Glu165 interaction shows weak hydrogen bonding on the basis of distance of hydrogen bond interaction of Ligand-1 (sofosbuvir) with the Mpro. Mpro Cys144 residue showed an average bond distance of 2.9 Å (Fig. 6 A). All four bonds show an average bond distance fluctuation of 1.9-8.9 Å during the whole simulation time. In the second run of MD, the interaction of Ligand 1 and Cys144, Gly167, and Glu165 appeared at about an average bond distance of 2.9 Å, 3.1 Å, and 3.2 Å and average bond distance fluctuation is 1.9-8 Å, shown less stable interaction between sofosbuvir with Mpro (Fig. 6 A and B).

In contrast, GS-441524 (Ligand 2) exhibited stable binding with the Mpro, and showed interaction of Glu165 with an average hydrogen bond distance of 2.2 Å throughout the simulation time. The other residues like Ser189, Gly167, and Pro188, showed an average hydrogen bond distance between 2.9 Å, while average bond distance fluctuation is 1.9-4.7 Å, conferring stable interaction between GS-441524 and Mpro (Fig. 7 A and B). During simulation time, the standard reference ligand, N3 compound against Mpro protein, showed interaction with Glu165 and Ser189 with an average bond distance of 2.5 Å, conferring stable interaction between N3 and Mpro. However, the residue Pro188 and Asn25 also exhibited an average hydrogen bond distance of 2.8 Å (Fig. 8 A and B).

4. Discussion

Feline infectious peritonitis (FIP) causes various clinical syndromes in the affected cats, caused by the feline infectious peritonitis virus (FIPV), a variant of the feline coronavirus (FCoV). Normally causing mild enteritis, FCoV transforms into FIPV, affecting multiple organs in cats (Sherding, 2009). The FIPV is an enveloped, positive-sense, single-stranded RNA virus classified within the Coronaviridae family, which also includes viruses like SARS-CoV, MERS-CoV, and SARS-CoV-2. Among humans and animals, coronaviruses exhibit the presence of similar structurally related functional proteins, such as the Mpro, also known as 3CL protease (3CLpro), which plays a crucial role in viral replication (Theerawatanasirikul et al., 2020). In this study, **t**he initial phases of drug screening for Mpro inhibitors involve drug-likeness assessment of different chemical compounds with the help of various factors. In this context, various computer-aided approaches, such as Lipinski's Rule of Five, are commonly applied *(Jia et al., 2020; Ahmad et al., 2024).*

The LogP values of all the compounds (Table 1), suggested that these compounds are likely to be more hydrophilic and may have better solubility in water, which can be beneficial for certain therapeutic applications where high aqueous solubility is required. This low LogP also indicates favorable hydrophobicity, contributing to increased persistence and bioavailability by reducing renal excretion *(Alvi et al., 2017)*.

In drug discovery, an MPSA value of ≤ 140 Å² is often considered an optimal threshold for oral bioavailability *(Veber et al., 2002)*. Drugs with higher MPSA values are less lipid-soluble and distributed less extensively, attributed to their less extensive and slower absorption rate than drugs with lower TPSA values. All the nucleoside analogs and precursors were showing below-threshold MPSA values. As a result, these compounds exhibit enhanced bioavailability and improved pharmacological efficiency. Based on these findings, all the selected nucleoside precursors and analogs qualify the criteria for MPSA. Compounds showing slightly increased MPSA values (near threshold ≤ 140 Å²) can be considered for further drug screening evaluations.

In ADMET analysis, aqueous solubility refers to the ability of a compound to dissolve in water, which is crucial for the compound's absorption, bioavailability, and pharmacokinetic properties. The aqueous solubility of a drug influences how well it can be absorbed in the gastrointestinal tract and how effectively it can be distributed throughout the body. However, the compounds Mizoribine, 6-Azauridine, and Ribavirin show solubility level 5 (Table 1), indicating compounds are extremely soluble, conferring unsuitable drug likeliness of these compounds on the basis of the solubility parameter of ADMET. On the other hand, the blood-brain barrier (BBB) model predicts blood-brain penetration after oral administration. In our investigation, all 14 selected compounds showed low penetration values for BBB. The plasma protein binding of drug molecules can affect the efficiency of a drug because the bound fraction is temporarily shielded from metabolism. On the other hand, only the unbound fraction exhibits pharmacological effects. Drugs with extreme PPB reflect a low volume of distribution (Vd), long plasma half-lives (T1/2), and may incur lower hepatic and renal clearance *(Roberts et al., 2013; Gurevich 2013)*.

On the basis of the ADMET model-predicted PPB, the model predicted false PPB for all the compounds, which suggests that, according to the model, these compounds are not predicted to have significant plasma protein binding (Table 2). This implies that the compounds do not strongly interact with plasma proteins and remain largely in their free form, which could lead to greater bioavailability, easy distribution to tissues, reaching the site of action and enhanced therapeutic

effects. The intestinal absorption analysis prediction results showed that compounds with intestinal absorption levels of 0–2 indicate good to moderate absorption and enhanced bioavailability, linked to the pharmacological actions of nucleoside analogs (Table 2). In contrast, inhibitors like N3, Methotrexate, Mizoribine, Ribavirin, and 6-Azauridine, with an absorption level of 3, suggest poor intestinal absorption. However, a compound with less absorption is not directly correlated with its pharmacological potential.

Based on the CYP2D6 values and corresponding predictions, out of 14 compounds, none of these drugs are expected to strongly interact with the CYP2D6 enzyme. Similarly, Mpro-standard inhibitor N3 also did not inhibit the CYP2D6 activity. Therefore, they are likely neither inhibitors nor substrates for CYP2D6, which may reduce the risk of metabolic interference. These results imply that the selected nucleoside analogs are likely to undergo rapid metabolism and excretion, potentially contributing to their potent pharmacological effects and reduced toxicity. CYP2D6 is involved in the metabolism of a wide range of substrates in the liver, and its inhibition by a drug constitutes a majority of cases of drug-drug interaction and mediates around 25 % of the total metabolism and clearance of the drugs after administration *(Ahmad et al., 2024)*. Furthermore, the toxicity assessment of nucleoside precursor and analogs results concluded that the Ames test predicts 6-Azauridine, Galidesivir, and Tenofovir as mutagenic, while the remaining compounds are non-mutagenic. The negative hepatotoxicity and Ames test values suggest that most compounds are less toxic and safe from mutagenic effects (Table 2). In conclusion, the drug likeliness and ADMET properties prediction results suggested that the selected nucleoside precursors and analogs may exhibit instant metabolism and excretion, which might be attributed to their substantial pharmacological effects as well as low toxicity.

Further, the molecular docking analysis of all selected compounds was conducted to identify potential anti-FIPV agents from a pool of nucleoside precursors and analogs. Using CDOCKER for molecular docking, we evaluated and ranked the binding affinities of promising compounds with the catalytic dyad residues (His41 and Cys144) in the binding pocket of FIPV-Mpro. The binding affinity from CDOCKER scores of the four top-ranked compounds and Mpro structure ranged from −46.7 to −12.2 (Table 3). These five top-ranked compounds were selected to calculate ΔG through the calculate binding energy method. The binding energy scores of 4 top-ranked complexes between ligands and the Mpro ranged between -13 to -10 kcal/mol (Table 3). Out of 14

selected compounds, the top four compounds that exhibited better binding affinity in catalytic dyad pockets are Sofosbuvir, Methotrexate, Pentoxifylline, and Molnupiravir. The CDOCKER and binding energy scores of reference ligand N3 with Mpro in the same binding pocket were 88.21 and -6.2 kcal/mol. The binding score and energy of all the compounds, including the reference ligand (N3) with FIPV-Mpro (Table 3). The interaction of N3 establishes interaction with Mpro through binding with specific residues Cys-144 and His-41 of the catalytic dyad of Mpro protein. Most interestingly, the residues stabilizing the binding of top-scoring nucleoside analog (sofosbuvir) against FIPV-Mpro were slightly different than that of other top-scoring nucleoside analogs and precursors (Methotrexate, Pentoxifylline, and Molnupiravir) suggesting that these potent inhibitors of FIPV-Mpro can be used synergistically to produce enhanced synergistic protective effects against FIPV infection via restricting the proteolysis of polyproteins and thereby restricting the expression of FIPV viral proteins/enzymes. The catalytic dyad residues Cys-144 and His-41 play a crucial role in Mpro enzymatic activity, facilitating the cleavage of viral polyproteins into functional proteins essential for viral replication *(Jin et al., 2020)*. This catalytic dyad is pivotal for the enzymatic activity of Mpro, facilitating the cleavage of viral polyproteins into functional proteins essential for viral replication and assembly *(Galasiti Kankanamalage et al., 2018; Jin et al., 2020)*. After the hijacking of the host's transcriptional machinery, Coronaviruses promote host cells to synthesize two overlapping polyproteins, pp1a and pp1ab, which cleave through coronavirus-encoded proteases—papain-like protease (PL^{pro}) and Mpro. The cleavage of pp1a and pp1ab forms 16 non-structural proteins, which play a role in viral replication *(Lu et al., 2022)*. Owing to the determining role in the proteolysis of viral polyproteins, the Mpro of the FIPV has been established as the preferred target in combating its virulence. Similarly, we also used FIPV-Mpro as the major target via selected nucleoside analogs for the management of this highly lethal infectious virus of domestic cats.

The stability of the interaction of ligands with the Mpro docking complexes was further investigated through MD simulation parameters. The RMSD was analyzed to assess the variations in the backbone Cα atoms of target proteins resulting from the binding of top-ranking nucleoside precursors and analogs along with their respective reference standards (N3). Ideally, RMSD values would be zero; however, due to statistical uncertainties, it is not possible for a protein to have an RMSD of zero *(Ahmad et al., 2024)*. The RMSD plots of each complex clearly demonstrate that all tested compounds–Mpro complexes show low RMSD values (RMSD < 2 Å), confirming the

stability of complexes during the simulation time when compared to the standard N3-Mpro complex (Fig. 2). The RMSD played a significant role in protein stability *(Elengoe et al., 2014)*.

Unlike RMSD, the Residual fluctuations in the MD simulation complexes were observed by Root Mean Square Fluctuation (RMSF) *(Ashraf et al., 2016)*. The RMSF is also defined as the standard measure of deviation of a molecule from its initial position *(Swetha et al., 2016)*. The RMSF quantifies the overall structural deviations over time and measures the root mean square fluctuations of individual amino acid residues, providing insight into the dynamic behavior and flexibility of these residues during simulations. This analysis identifies critical residues contributing to conformational flexibility within the protein. This study performed a comprehensive RMSF analysis of the top ligand-protein complexes to evaluate the mobility of residues within the protein's active site. The fluctuations observed in the RMSF profiles throughout the simulation runs pinpointed regions of the protein undergoing significant motion. Investigation of the RMSF showed low or equal RMSF for all the complexes as compared to standard N3-Mpro complex (Fig. 3). In conclusion, it indicated that the RMSF of all complexes is significantly similar compared to reference, resulting in less fluctuation and good stability *(Mathpal et al., 2022)*.

However, the compactness of the target protein-ligand complex was measured through RG *(Abbas et al., 2017)*. The stability of the FIPV- Mpro with ligands exhibiting the best binding energies was further evaluated using the RG, which measures the protein's size and compactness *(Arnittali et al., 2019)*. The magnitude of RG inversely correlates with protein stability, where a larger RG indicates a less stable, more expanded structure. The RG value GS-441524 -Mpro complex was 0.2-0.4 Å low, comparable to that of the N3-Mpro complex. However, the RG value of the Sofosbuvir-Mpro complex was similar to the N3-Mpro complex over the 50,000 ps simulation, suggesting that the protein is less compact and denser upon complex formation (Fig. 4). In conclusion, the higher RG value attributed to the low compactness of the ligand-protein complex. This indicates that GS-441524-Mpro and Sofosbuvir-Mpro complexes demonstrated significant structural compactness and stability. If the protein is likely to maintain a relatively steady value of RG over the MD simulation, it is regarded as s folded and more stable. If its RG changes over time, it would be considered unfolded *(Ghasemi et al., 2016)*.

Further, a number of hydrogen bond establishments and changes in the distance of the compounds to the amino acid residues contributing to substantial hydrogen bonds were assessed by studying the variation of distance between Ca atoms of the binding cavity and the compounds throughout the

MD simulations. In the simulation result, the average number of hydrogen bond establishment and hydrogen bond distance between the compounds and the contributing residues was shown by GS-441524-Mpro as compared to standard N3-Mpro, which is below 2.5 Å. During the MD simulations of the compound sofosbuvir (Ligand-1) and the distance between the compound and Mpro, both Ser189 and Val42 amino acid residues showed high fluctuations as compared to Standard N3 and GS-441524. While, compound GS-441524 (Ligand-2) and Mpro interacted residues showed less fluctuation for hydrogen bond distance (Fig. 7), as compared to standard N3-Mpro and (Fig. 8) and Ligand-1 Sofosbuvir-Mpro interacted residues (Fig. 6). More fluctuation in hydrogen bond distance attributed to the less effective binding of ligand with residues of active pocket of protein *(Rasyid et al., 2021).* The average distance between the compounds and the hydrogen bond contributing residues should be near or below 2.5 Å, which falls within the accepted range *(Nada et al., 2022).* The residues stabilizing the binding of compounds exhibiting low hydrogen bond distance (GS-441524 and Sofosbuvir) against FIPV-Mpro were different than that of top-scoring residues of reference standard N3, suggesting that these potent inhibitors can be used synergistically to produce enhanced synergistic protective effects against FIPV infection via restricting the proteolysis of polyproteins and related expression of viral proteins. Restricting the expression of viral proteins/enzymes as a combinatorial effect of compounds is reported for SARS-CoV-2 inhibition *(Ullrich & Nitsche, 2020; Keretsu et al., 2020)*. Therefore, the docking analysis findings and different MD simulation parameters, including hydrogen bond distance analysis compared with the N-Mpro complex, validate the GS-441524 as an FIPV-Mpro inhibitor.

Gilead Science (GS)-441524 is a 10-cyano adenosine analog, which is the main plasma metabolite of the more famous antiviral drug remdesivir *(Amirian and Levy, 2020).* Several cellular studies conducted on GS-441524 indicated an anti-SARS-CoV-2 activity comparable when not higher than Rremdesivir (Yan & Muller, 2020), with some studies pointing out that GS-441524 would be even more convenient than Remdesivir for the COVID-19 therapy (Yan & Muller, 2020), GS-441524 advantages over Remdesivir include ease of synthetic preparation, lower hepatic toxicity, as well as oral administration route (not suitable for Remdesivir due to its poor liver stability) (Yan & Muller, 2020). However, Sofosbuvir is also a nucleoside analog used to treat HCV infection, which can inhibit the SARS-CoV-1 RNA-dependent RNA polymerase, affecting the viral life cycle *(Jácome et al., 2020; Seyed et al., 2020)*. Sofosbuvir-based treatment regimens may help to reduce the mortality of patients with SARS-CoV-2 and improve associated complications

(Hsu et al., 2022). Sofosbuvir is a prodrug that is hydrolyzed by liver enzymes after absorption to form the monophosphate uridine analog, which is further phosphorylated to form the active triphosphate form *(Alrehaily et al., 2023)*.

The docking study, GS-441524 interaction could inhibit its binding with polyproteins, pp1a and pp1ab. Our docking and molecular dynamic simulation study parameters confirm that developing a single antiviral agent targeting Mpro suggests GS-441524 either used as a drug alone in treatment or in combination with other potential therapies. This could serve as a potential system that could pave the way to defend against diseases associated with animal coronaviruses. Additionally, our findings provide valuable insights for advancing the development of antiviral agents and broadening the range of anti-CoV agents available for combating feline coronavirus and other related coronaviruses.

5. Conclusions:

The results from this study support the development of a single antiviral agent GS-441524, Mpro targeting agent, and its combination with other potential therapies could provide an effective first line of defense against diseases associated with feline coronaviruses. Further, our findings offer essential insights for further developing antiviral agents and expanding the reservoir of anti-FIPV agents for targeting feline coronavirus and other related coronaviruses. Nevertheless, this initial in-silico study should be validated through in-vitro and in-vivo experiments in infection models. Additionally, the predicted binding affinity profiles, stability analysis, and ADME and toxicity of the selected nucleoside precursors and analogs based on algorithm-based tools and approaches may vary in experimental settings.

Acknowledgments

This study was funded by a seed grant from Long Island University (Grant no: 36524).

Conflicts of interest

The authors declare no conflicts of interest.

References:

Abbas Q, Ashraf Z, Hassan M, Nadeem H, Latif M, Afzal S, Seo SY. 2017. Development of highly potent melanogenesis inhibitor by in vitro, in vivo and computational studies. *Drug Design, Development and Therapy* 11:2029-46. https://doi.org/10.2147/DDDT.S137550

Addie DD, Covell-Ritchie J, Jarrett O, Fosbery M. 2020. Rapid resolution of non-effusive feline infectious peritonitis uveitis with an oral adenosine nucleoside analogue and feline interferon omega. *Viruses* 12(11):1216. https://doi.org/10.3390/v12111216

Agu PC, Afiukwa CA, Orji OU, Ezeh EM, Ofoke IH, Ogbu CO, Ugwuja EI, Aja PM. 2023. Molecular docking as a tool for the discovery of molecular targets of nutraceuticals in diseases management. *Scientific Reports* 13(1):13398. DOI: DOI:10.1038/s41598-023-40160-2

Ahmad P, Alvi SS, Iqbal J, Khan MS. 2021. Identification and evaluation of natural organosulfur compounds as potential dual inhibitors of α-amylase and α-glucosidase activity: an in-silico and in-vitro approach. *Medicinal Chemistry Research* 30:2184-2202. https://doi.org/10.1007/s00044-021-02799-2

Ahmad P, Alvi SS, Hasan I, Khan MS. 2024. Targeting SARS-CoV-2 main protease (Mpro) and human ACE-2: A virtual screening of carotenoids and polyphenols from tomato (Solanum lycopersicum L.) to combat Covid-19. *Intelligent Pharmacy* 2(1):51-68. https://doi.org/10.1016/j.ipha.2023.10.008

Ali MR, Kumar S, Afzal O, Shalmali N, Ali W, Sharma M, Bawa S. 2017. 2-Benzamido-4-methylthiazole-5-carboxylic Acid Derivatives as Potential Xanthine Oxidase Inhibitors and Free Radical Scavengers. *Archiv der Pharmazie* 350(2):1600313. https://doi.org/10.1002/ardp.201600313

Alrehaily A, Elfiky AA, Ibrahim IM, Ibrahim MN, Sonousi A. 2023. Novel sofosbuvir derivatives against SARS-CoV-2 RNA-dependent RNA polymerase: an in silico perspective. *Scientific Reports*13(1):23080. https://doi.org/10.1038/s41598-023-49712-y

Alvi SS, Ansari IA, Ahmad MK, Iqbal J, Khan MS. 2017. Lycopene amends LPS induced oxidative stress and hypertriglyceridemia via modulating PCSK-9 expression and Apo-CIII mediated lipoprotein lipase activity. *Biomedicine & Pharmacotherapy* 96:1082-93. https://doi.org/10.1016/j.biopha.2017.11.116

Amirian ES, Levy JK. 2020. Current knowledge about the antivirals remdesivir (GS-5734) and GS-441524 as therapeutic options for coronaviruses. *One Health* 9, 100128. [CrossRef]

Arnittali M, Rissanou AN, Harmandaris V. 2019. Structure of biomolecules through molecular dynamics simulations. *Procedia Computer Science* 156:69-78. https://doi.org/10.1016/j.procs.2019.08.181

Ashraf Z, Alamgeer, Rasool R, Hassan M, Ahsan H, Afzal S, Afzal K, Cho H, Kim SJ. 2016. Synthesis, bioevaluation and molecular dynamic simulation studies of dexibuprofen–antioxidant mutual prodrugs. *International Journal of Molecular Sciences* 17(12):2151. https://doi.org/10.3390/ijms17122151

584 Brierley I, Digard P, Inglis SC 1989. Characterization of an efficient coronavirus ribosomal
585 frameshifting signal: requirement for an RNA pseudoknot. *Cell* 57(4):537-47.
586 https://doi.org/10.1016/0092-8674(89)90124-4

587 Bultum LE, Tolossa GB, Kim G, Kwon O, Lee D. 2022. In silico activity and ADMET profiling
588 of phytochemicals from Ethiopian indigenous aloes using pharmacophore models. *Scientific*
589 *Reports* 12(1):22221. https://doi.org/10.1038/s41598-022-26446-x

590 Chu CS, Simpson JD, O'Neill PM, Berry NG. 2021. Machine learning–Predicting Ames
591 mutagenicity of small molecules. *Journal of Molecular Graphics and Modelling* 109:108011.
592 https://doi.org/10.1016/j.jmgm.2021.108011

593 Dedeurwaerder A, Desmarets LM, Olyslaegers DA, Vermeulen BL, Dewerchin HL,
594 Nauwynck HJ. 2013. The role of accessory proteins in the replication of feline infectious
595 peritonitis virus in peripheral blood monocytes. *Veterinary microbiology* 162(2-4):447-55.
596 https://doi.org/10.1016/j.vetmic.2012.10.032

597 Dickinson PJ, Bannasch M, Thomasy SM, Murthy VD, Vernau KM, Liepnieks M,
598 Montgomery E, Knickelbein KE, Murphy B, Pedersen NC. 2020. Antiviral treatment using the
599 adenosine nucleoside analogue GS-441524 in cats with clinically diagnosed neurological
600 feline infectious peritonitis. *Journal of veterinary internal medicine* 34(4):1587-93.
601 https://doi.org/10.1111/jvim.15780

602 Ding X, Wu Y, Wang Y, Vilseck JZ, Brooks III CL. 2020. Accelerated CDOCKER with
603 GPUs, parallel simulated annealing, and fast Fourier transforms. *Journal of chemical theory*
604 *and computation* 16(6):3910-9. https://doi.org/10.1021/acs.jctc.0c00145

605 Egan WJ, Lauri G. 2002. Prediction of intestinal permeability. *Advanced drug delivery reviews*
606 54(3):273-89. https://doi.org/10.1016/s0169-409x(02)00004-2

607 Elengoe A, Naser MA, Hamdan S. 2014. Modeling and docking studies on novel mutants
608 (K71L and T204V) of the ATPase domain of human heat shock 70 kDa protein 1. *International*
609 *Journal of Molecular Sciences* 15(4):6797-814. https://doi.org/10.3390/ijms15046797

610 Gagnon JK, Law SM, Brooks III CL. 2016. Flexible CDOCKER: Development and
611 application of a pseudo-explicit structure-based docking method within CHARMM. *Journal*
612 *of computational chemistry* 37(8):753-62. https://doi.org/10.1002/jcc.24259

613 Kankanamalage AC, Kim Y, Damalanka VC, Rathnayake AD, Fehr AR, Mehzabeen N,
614 Battaile KP, Lovell S, Lushington GH, Perlman S, Chang KO. 2018. Structure-guided design
615 of potent and permeable inhibitors of MERS coronavirus 3CL protease that utilize a piperidine
616 moiety as a novel design element. *European journal of medicinal chemistry* 150:334-46.
617 https://doi.org/10.1016/j.ejmech.2018.03.004

618 Ghasemi F, Zomorodipour A, Karkhane AA, Khorramizadeh MR. 2016. In silico designing of
619 hyper-glycosylated analogs for the human coagulation factor IX. *Journal of Molecular*
620 *Graphics and Modelling* 68:39-47. https://doi.org/10.1016/j.jmgm.2016.05.011

621 Gurevich KG. 2013. Effect of blood protein concentrations on drug-dosing regimes: practical
622 guidance. *Theoretical Biology and Medical Modelling* 10:1-7. https://doi.org/10.1186/1742-
623 4682-10-20

624 Hohdatsu T, Okada S, Koyama H. 1991. Characterization of monoclonal antibodies against
625 feline infectious peritonitis virus type II and antigenic relationship between feline, porcine, and
626 canine coronaviruses. *Archives of virology* 117:85-95. https://doi.org/10.1007/bf01310494

627 Hsu CK, Chen CY, Chen WC, Lai CC, Hung SH, Lin WT. 2022. Effect of sofosbuvir-based
628 treatment on clinical outcomes of patients with COVID-19: a systematic review and meta-
629 analysis of randomised controlled trials. *International Journal of Antimicrobial Agents*
630 59(3):106545. https://doi.org/10.1016/j.ijantimicag.2022.106545

631 Jácome R, Campillo-Balderas JA, Ponce de León S, Becerra A, Lazcano A. 2020. Sofosbuvir
632 as a potential alternative to treat the SARS-CoV-2 epidemic. *Scientific Reports* 10(1):9294.
633 https://doi.org/10.1038/s41598-020-66440-9

634 Jaimes JA, Whittaker GR. 2018. Feline coronavirus: Insights into viral pathogenesis based on
635 the spike protein structure and function. *Virology* 517:108-21.
636 https://doi.org/10.1016/j.virol.2017.12.027

637 Jia CY, Li JY, Hao GF, Yang GF. 2020. A drug-likeness toolbox facilitates ADMET study in
638 drug discovery. *Drug discovery today* 25(1):248-58.
639 https://doi.org/10.1016/j.drudis.2019.10.014

640 Jin Z, Du X, Xu Y, Deng Y, Liu M, Zhao Y, Zhang B, Li X, Zhang L, Peng C, Duan Y. 2020.
641 Structure of Mpro from SARS-CoV-2 and discovery of its inhibitors. *Nature* 582(7811):289-
642 93. https://doi.org/10.1038/s41586-020-2223-y

643 Kato H. 2020. Computational prediction of cytochrome P450 inhibition and induction. *Drug*
644 *metabolism and pharmacokinetics* 35(1):30-44. https://doi.org/10.1016/j.dmpk.2019.11.006

645 Kennedy MA. 2020. Feline infectious peritonitis: update on pathogenesis, diagnostics, and
646 treatment. *Veterinary Clinics: Small Animal Practice* 50(5):1001-11.
647 https://doi.org/10.1016/j.cvsm.2020.05.002

648 Keretsu S, Bhujbal SP, Cho SJ. 2020. Rational approach toward COVID-19 main protease
649 inhibitors via molecular docking, molecular dynamics simulation and free energy calculation.
650 *Scientific reports* 10(1):17716. https://doi.org/10.1038/s41598-020-74468-0

651

652 Lu J, Chen SA, Khan MB, Brassard R, Arutyunova E, Lamer T, Vuong W, Fischer C, Young
653 HS, Vederas JC, Lemieux MJ. 2022. Crystallization of feline coronavirus Mpro with GC376
654 reveals mechanism of inhibition. *Frontiers in Chemistry* 10:852210**.**
655 **https://doi.org/10.3389/fchem.2022.852210**

656 Mathpal S, Joshi T, Sharma P, Joshi T, Pundir H, Pande V, Chandra S. 2022. A dynamic
657 simulation study of FDA drug from zinc database against COVID-19 main protease receptor.
658 *Journal of Biomolecular Structure and Dynamics* 40(3):1084-100.
659 DOI:10.1080/07391102.2020.1821785

660 Meng XY, Zhang HX, Mezei M, Cui M. 2011. Molecular docking: a powerful approach for
661 structure-based drug discovery. *Current computer-aided drug design* 7(2):146-57.
662 https://doi.org/10.2174/157340911795677602

663 Murphy BG, Perron M, Murakami E, Bauer K, Park Y, Eckstrand C, Liepnieks M, Pedersen
664 NC. 2018. The nucleoside analog GS-441524 strongly inhibits feline infectious peritonitis
665 (FIP) virus in tissue culture and experimental cat infection studies. *Veterinary microbiology*
666 219:226-33. https://doi.org/10.1016/j.vetmic.2018.04.026

667 Nada H, Elkamhawy A, Lee K. 2022. Identification of 1H-purine-2, 6-dione derivative as a
668 potential SARS-CoV-2 main protease inhibitor: molecular docking, dynamic simulations, and
669 energy calculations. *PeerJ* 10:e14120. https://doi.org/10.7717/peerj.14120

670 Pedersen NC, Perron M, Bannasch M, Montgomery E, Murakami E, Liepnieks M, Liu H.
671 2019. Efficacy and safety of the nucleoside analog GS-441524 for treatment of cats with
672 naturally occurring feline infectious peritonitis. *Journal of feline medicine and surgery*
673 21(4):271-81. https://doi.org/10.1177/1098612x19825701

674 Rasyid H, Purwono B, Pranowo HD. 2021. Design of new quinazoline derivative as EGFR
675 (Epidermal growth factor receptor) inhibitor through molecular docking and dynamics
676 simulation. *Indonesian Journal of Chemistry* 21(1):201-11. https://doi.org/10.22146/ijc.57012

677 Roberts JA, Pea F, Lipman J. 2013. The clinical relevance of plasma protein binding changes.
678 *Clinical pharmacokinetics* 52:1-8. https://doi.org/10.1007/s40262-012-0018-5

679 Santos, R., et al., 2017. Bayesian models for predicting CYP2D6 inhibition. *Journal of*
680 *Medicinal Chemistry* 60(2): 672–684. DOI: 10.1021/acs.jmedchem.6b01073.

681 Schmied K, Ehmann R, Kristen-Burmann C, Ebert N, Barut GT, Almeida L, Kelly JN,
682 Thomann L, Stalder H, Lang R, Tekes G. 2024. An RNA replicon system to investigate
683 promising inhibitors of feline coronavirus. *Journal of virology* 98(2):e01216-23.
684 https://doi.org/10.1128/jvi.01216-23

Hosseini ES, Kashani NR, Nikzad H, Azadbakht J, Bafrani HH, Kashani HH.2020. The novel coronavirus Disease-2019 (COVID-19): Mechanism of action, detection and recent therapeutic strategies. *Virology* 551:1-9. https://doi.org/10.1016/j.virol.2020.08.011

Sherding RG. 2009. Feline infectious peritonitis (feline coronavirus). *Saunders Manual of Small Animal Practice* 15:132. https://doi.org/10.1016/B0-72-160422-6/50012-7

Swetha RG, Ramaiah S, Anbarasu A. 2016. Molecular dynamics studies on D835N mutation in FLT3—its impact on FLT3 protein structure. *Journal of Cellular Biochemistry* 117(6):1439-45. https://doi.org/10.1002/jcb.25434

Theerawatanasirikul S, Kuo CJ, Phecharat N, Chootip J, Lekcharoensuk C, Lekcharoensuk P. 2020. Structural-based virtual screening and in vitro assays for small molecules inhibiting the feline coronavirus 3CL protease as a surrogate platform for coronaviruses. *Antiviral research* 182:104927. https://doi.org/10.1016/j.antiviral.2020.104927

Ullrich S, Nitsche C. 2020. The SARS-CoV-2 main protease as drug target. *Bioorganic & medicinal chemistry letters* 30(17):127377. https://doi.org/10.1016/j.bmcl.2020.127377

Veber DF, Johnson SR, Cheng HY, Smith BR, Ward KW, Kopple KD. 2002. Molecular properties that influence the oral bioavailability of drug candidates. *Journal of medicinal chemistry* 45(12):2615-23. https://doi.org/10.1021/jm020017n

Wang YC, Yang WH, Yang CS, Hou MH, Tsai CL, Chou YZ, Hung MC, Chen Y. 2020. Structural basis of SARS-CoV-2 main protease inhibition by a broad-spectrum anti-coronaviral drug. *American journal of cancer research* 10(8):2535. https://pmc.ncbi.nlm.nih.gov/articles/PMC7471349/

Yan V. Muller F. 2020. Comprehensive Summary Supporting Clinical Investigation of GS-441524 for Covid-19 Treatment. *OSF Preprints*. https://doi.org/10.31219/osf.io/mnhxu.

Figure legends:

Figure 1: The best docking hit pose of GS-441524, sofosbuvir, and reference standard (N3) with the Mpro. (A), (B), and (C) show 3D docking poses of the standard N3 (sea blue), compound Sofosbuvir (green), and GS-441524 interaction with residues of the binding cavity of FIPV-Mpro, respectively. (D) The top hit of GS-441524 (red) and sofosbuvir (green) overlayed on the top pose of reference standard N3 (sea blue) inside the binding cavity of Mpro protein.

Figure 2. The RMSD profile values for the backbone atoms of the standard inhibitor Standard (N3)-Mpro and protein-ligand complexes of Sofosbuvir (Ligand-1)-Mpro and GS-441524 (Ligand-2)-Mpro from initial structures to complete MD simulation period.

Figure 3. The RMSF of the Standard (N3)-Mpro, Sofosbuvir (Ligand-1)-Mpro, and GS-441524 (Ligand-2)-Mpro complexes during 50,000 ps simulation.

Figure 4. The radius of gyration of the Standard (N3)-Mpro, Sofosbuvir (Ligand-1)-Mpro, and GS-441524 (Ligand-2)-Mpro complexes during 50,000 ps simulation. The plot of the Radius of Gyration reflects the changes observed in the conformational behavior of all protein-ligand complexes compared with the standard complex (N-Mpro).

Figure 5. Hydrogen bond (Hbond) monitor plots showed the number of hydrogen bonds established during 50,000 picosecond simulation time. (A and C) A hydrogen bond occurs between Mpro-protein and Ligand-1 (Sofosbuvir) in MD's first and second run. (B and D) A hydrogen bond occurs between Mpro-protein and Ligand-2 (GS-441524) in MD's first and second run. (E and F) Hydrogen bond occurs between Mpro-protein and Standard (N3) in the first and second run of MD.

Figure 6. The hydrogen bond distance plot of compound Sofosbuvir (Ligand-1) with Mpro protein. (A and B) The plot indicates changes in distance between key binding-site amino acids and the ligands over time during each run of MD simulation.

Figure 7. The hydrogen bond distance plot of compound GS-441524 (Ligand-2) with Mpro protein. (A and B) The plot indicates changes in distance between key binding-site residues and the ligands over time during each run of MD simulation.

Figure 8. The hydrogen bond distance plot of compound N3 (standard) with Mpro protein. (A and B) The plot indicates changes in distance between key binding-site amino acids and the ligands over time during each run of MD simulation.

Table 1(on next page)

Table 1. Chemical properties of selected nucleoside precursors and analogs

Chemical properties of selected nucleoside precursors and analogs

Table 1. Summary of the chemical properties of selected nucleoside precursors and analogs

S.N.	Compound name	Pubchem iD (CID)	M.WT	ALogP	HBA	HBD	LPV	MPSA (Å²)
1	6-Azauridine	5901	245.189	-2.432	9	4	0	131.69
2	Baricitinib	44205240	371.417	0.36	9	1	0	128.94
3	Favipiravir	492405	157.103	-1.392	5	2	0	84.55
4	Gemcitabine	60750	263.198	-1.394	7	3	0	108.37
5	GS-441524	44468216	291.263	-1.43	9	4	0	149.91
6	Molnupiravir	145996610	329.306	-0.875	10	4	0	140.91
7	Oxipurinol	135398752	152.111	-0.867	6	3	0	86.88
8	Pentoxifylline	4740	278.307	0.507	7	0	0	75.51
9	Ribavirin	37542	244.205	-2.745	9	4	0	143.72
10	Tenofovir	464205	287.212	-0.772	9	3	0	146.19
11	Galidesivir	10445549	265.269	-1.582	8	7	1	140.31
12	Methotrexate	126941	454.439	0.114	13	7	2	210.53
13	Mizoribine	104762	259.216	-2.409	9	6	1	151.06
14	Sofosbuvir	45375808	529.453	0.921	12	3	2	152.54
15	*N3	146025593	680.791	3.54	14	6	3	204.74

* Represents the reference standard inhibitor of FIPV-Mpro activity. M.WT.: Molecular Weight; HBD: Hydrogen bond doner; HBA: Hydrogen bond acceptors; MPSA: Molecular polar surface area; LPV: Lipinski Violation

Table 2(on next page)

Table. 2. Predicted ADME properties and toxicity of selected nucleoside precursors and analogs.

Predicted ADME properties and toxicity of selected nucleoside precursors and analogs.

Table 2. Summary of the predicted ADME properties and toxicity of selected nucleoside precursors and analogs.

S.N.	Compounds	Solubility level	BBB level	CYP2D6 prediction	Hepatoxicity prediction	Absorption level	PPB prediction	TOPTAK AMES prediction
1	*N3	3	4	false	false	3	false	Non-Mutagen
2	6-Azauridine	5	4	false	true	3	false	Mutagen
3	Baricitinib	3	4	false	true	0	false	Non-Mutagen
4	favipiravir	4	4	false	true	1	false	Non-Mutagen
5	Galidesivir	4	4	false	true	2	false	Mutagen
6	Gemcitabine	4	4	false	true	1	false	Non-Mutagen
7	GS-441524	4	4	false	true	2	false	Non-Mutagen
8	Methotrexate	2	4	false	true	3	false	Non-Mutagen
9	Mizoribine	5	4	false	true	3	false	Non-Mutagen
10	Molnupiravir	4	4	false	true	2	false	Non-Mutagen
11	Oxipurinol	4	3	false	true	0	false	Non-Mutagen
12	Pentoxifylline	3	3	false	false	0	false	Non-Mutagen
13	Ribavirin	5	4	false	true	3	false	Non-Mutagen
14	Sofosbuvir	3	4	false	true	3	false	Non-Mutagen
15	Tenofovir	4	4	false	true	1	false	Mutagen

* Represents the reference standard inhibitor of FIPV-Mpro. BBB: blood brain barrier; PPB: plasma protein binding

Table 3(on next page)

Table 3. FIPV-Mpro with ligand N3 interaction

Interacting pattern of various nucleoside precursors and analogs with crystal structure of FIPV-Mpro with ligand N3 (PDBID:5EU8)

Table 3: Summary of the interacting patterns of selected nucleoside precursors and analogs with crystal structure of FIPV-Mpro with ligand N3 (PDBID:5EU8)

S.No	Compounds	-CDOCk Energy	CDOCK Int Energy	Binding energy	MM-GBSA	Ligand interacting residues of Mpro
1	*N3	88.72	68.11	-7.11	-90.64	Asn25, His41, Ala141, Cys144 Leu164, Glu165, Leu166, Gly167, Pro188, Met190
2	Sofosbuvir	39.56	39.34	-7.38	-106.82	His41, Cys144, Leu164, Glu165, Leu166, Pro188
3	GS-441524	41.12	43	-7.2	-91.02	His41, Thr47, His162, His163, Leu164, Glu165, Pro188
4	Methotrexate	18.71	24.68	-6.98	-88.76	Thr47, Ala141, Leu164, Glu165, Pro188
5	Pentoxifylline	11.40	39.67	-6.65	-67.42	Thr47, Cys144, His162, Leu164, Pro188, Ser189
6	Molnupiravir	25.78	25.81	-6.60	-63.24	His163, Leu164, Pro188, Ser189
7	Tenofovir	-3.03	29.49	-6.4	-62.66	Thr47, His163, Leu164, Glu165, Lgn187, Pro188
8	6-Azauridine	0.16	26	-6.5	-54.72	Thr47, Cys144, His162, Glu165
9	Mizoribine	-12.90	18.30	-5.83	-70.64	Ser48, His163, Glu165, Pro188
10	Oxipurinol	0.45	14	-5.7	-35.16	His41, Thr47, His163, Leu164, Glu165
11	Galidesivir	-1.87	27.53	-4.59	-46.67	Thr47, Leu164, Glu165, Asp186
12	Favipiravir	8.77	16.91	-5.32	-45.49	Leu164, Asp186, Pro188
13	Barcitinib	-29	28	-5.13	-59.06	Cys144, Leu164, Pro188
14	Ribavirin	-19	22	-5.11	60.24	Thr47, Cys144, His163, Leu164, Pro188
15	Gemcitabine	12	28	-5.86	-63.37	Thr47, His163, Leu164, Pro188

* Represents the reference standard inhibitor of FIPV-Mpro activity. CDOCK Int Energy: CDOCKER Interaction energy

Figure 1

Figure-1. The best docking hit pose of sofosbuvir and reference standard N3 with the FIPV-Mpro.

The best docking hit pose of sofosbuvir and reference standard N3 with the FIPV-Mpro. (A) The top hit of sofosbuvir (green) overlayed on the top pose of reference standard N3 (sea blue) inside the binding cavity of Mpro protein. (B) and (C) showing 3D docking poses of the standard N3 (sea blue) and compound Sofosbuvir (green) interaction with residues of the binding cavity of FIPV-Mpro, respectively.

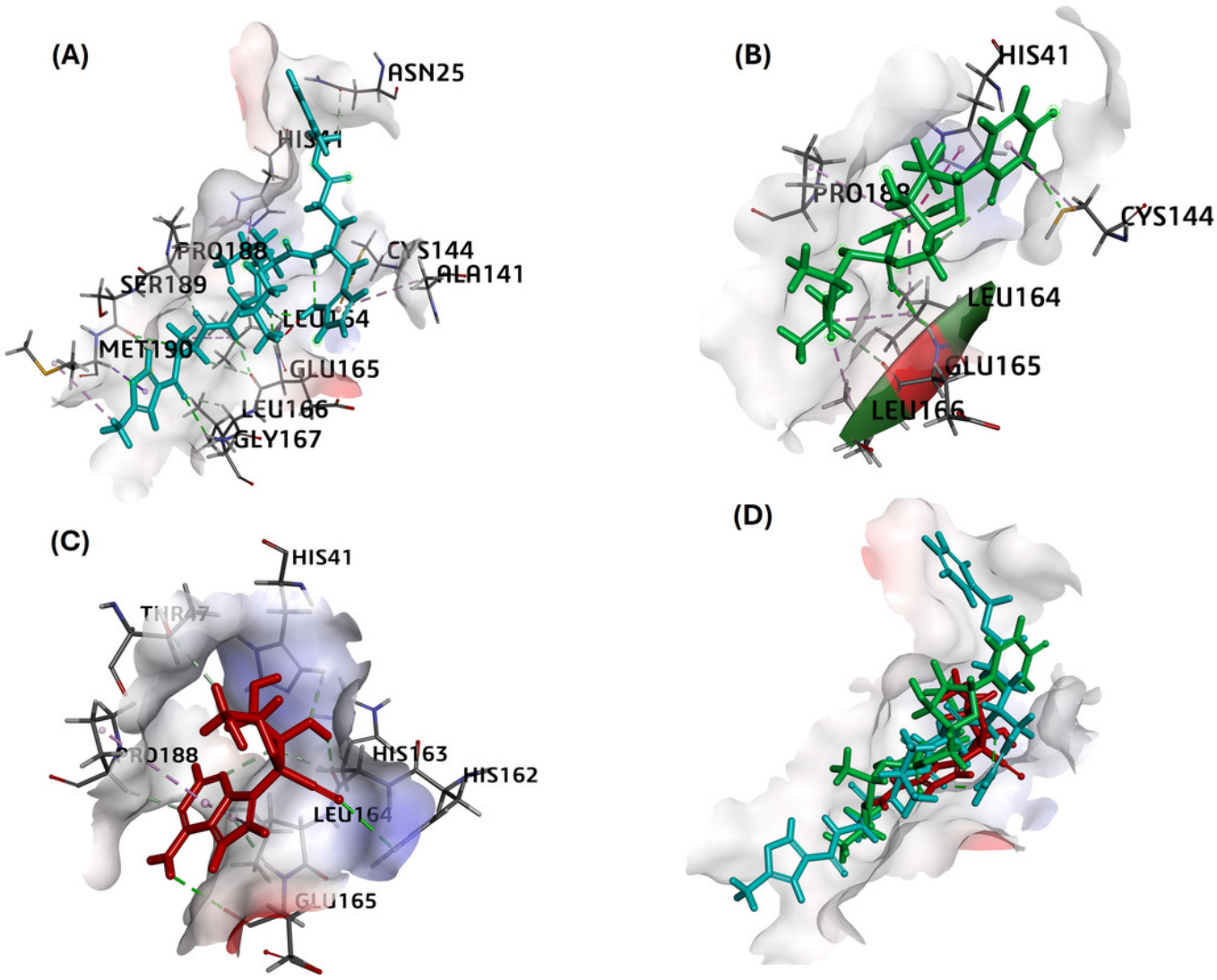

Figure 2

Figure 2. The RMSD profile values for the backbone atoms of the standard inhibitor N3-Mpro and all protein-ligand complexes

RMSD profile values for the backbone atoms of the standard inhibitor N3-Mpro and all protein-ligand complexes, including Molnupiravir-Mpro, Pentoxifylline-Mpro, Methotrexate-Mpro, and Sofosbuvir-Mpro from initial structures to complete MD simulation period.

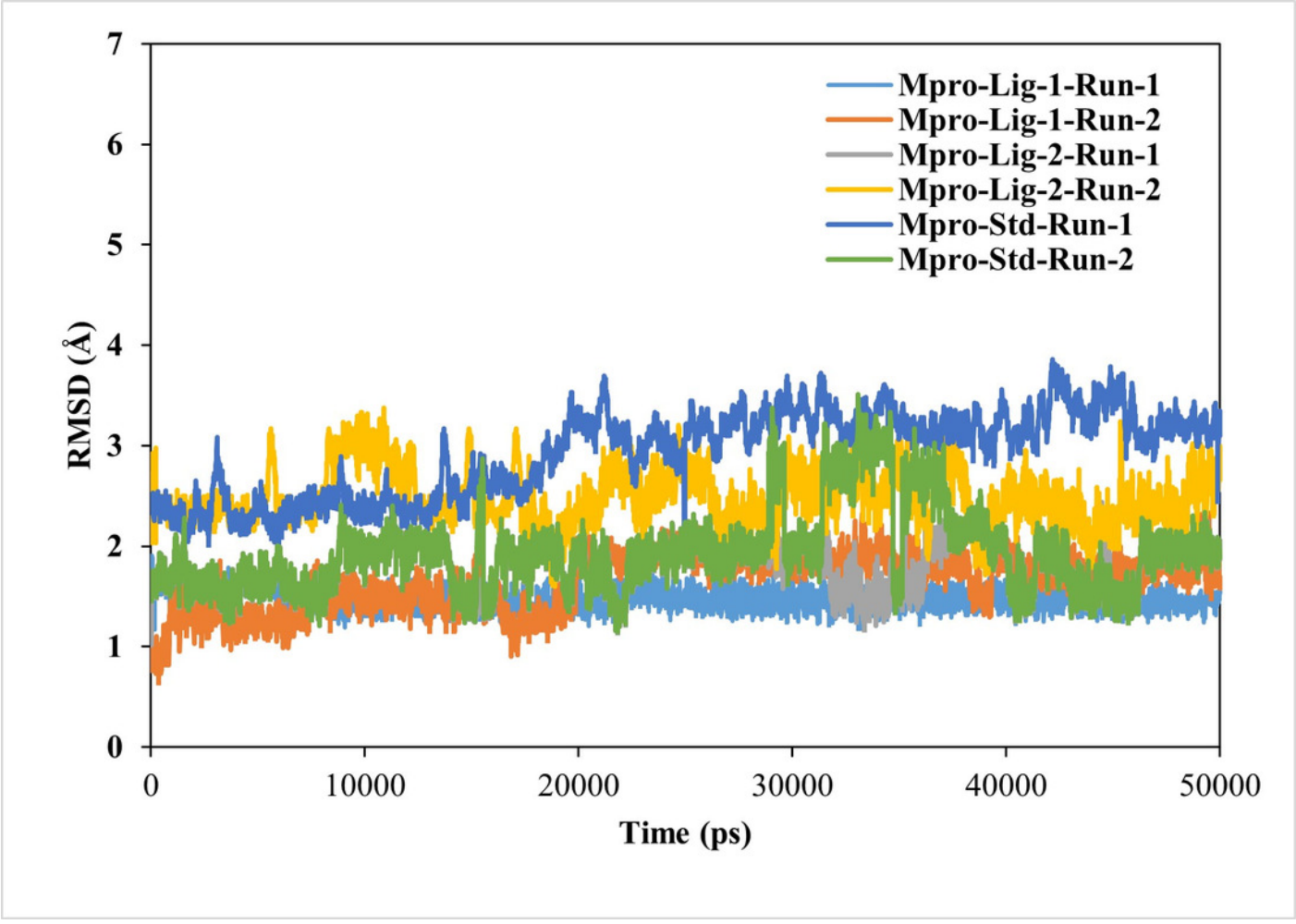

Figure 3

Figure 3. The RMSF of the N3-Mpro

The RMSF of the N3-Mpro, Molnupiravir-Mpro, Pentoxifylline-Mpro, Methotrexate-Mpro, and Sofosbuvir-Mpro complexes during complete simulation.

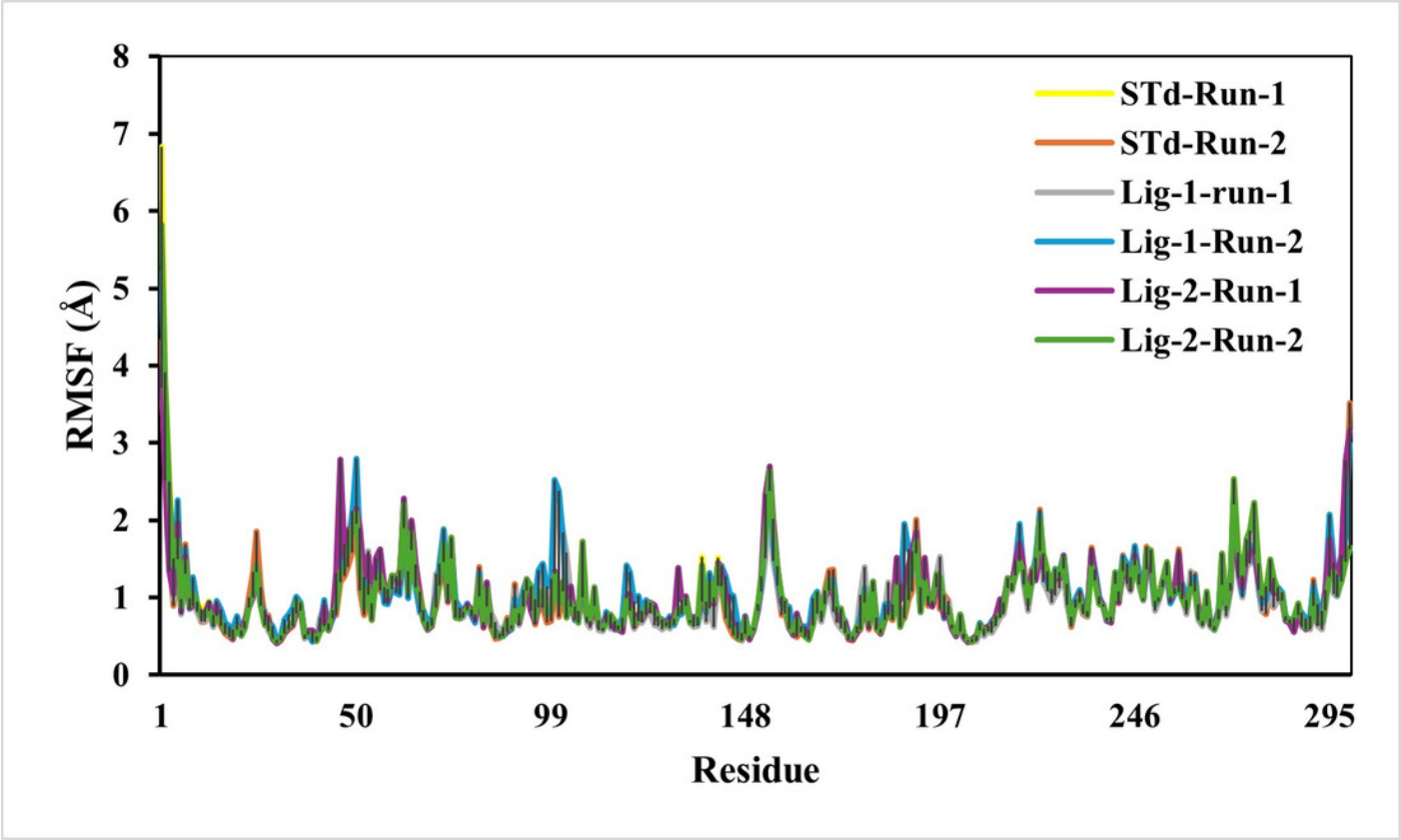

Figure 4

Figure 4. The RMSF of the N3-Mpro

The RMSF of the N3-Mpro, Molnupiravir-Mpro, Pentoxifylline-Mpro, Methotrexate-Mpro, and Sofosbuvir-Mpro complexes during complete simulation.

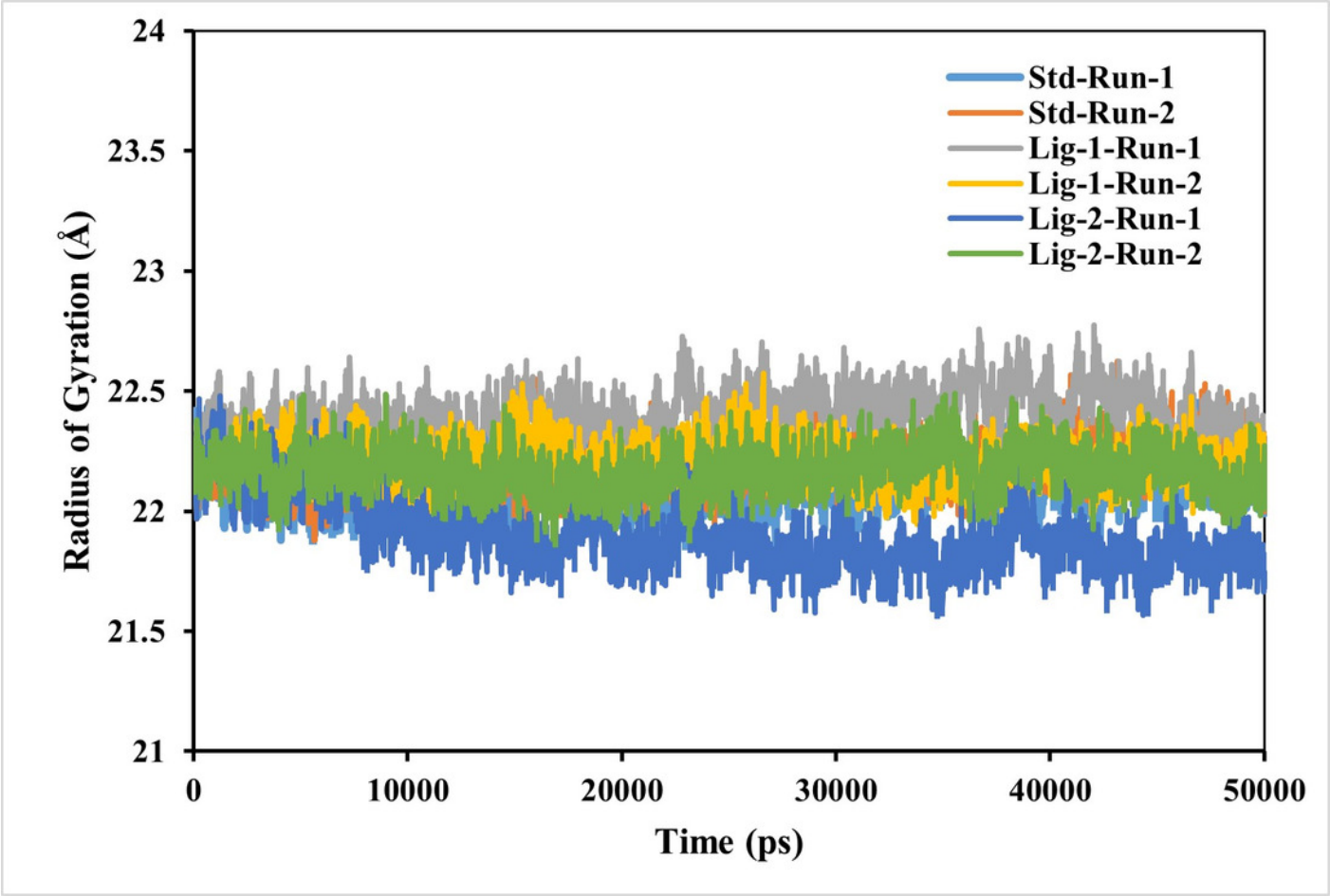

Figure 5

Figure 5. The hydrogen bond distance plot of compound Molnupiravir with Mpro protein

The plot indicates changes in the distance between key binding-site amino acids and the ligands over time during each MD simulation.

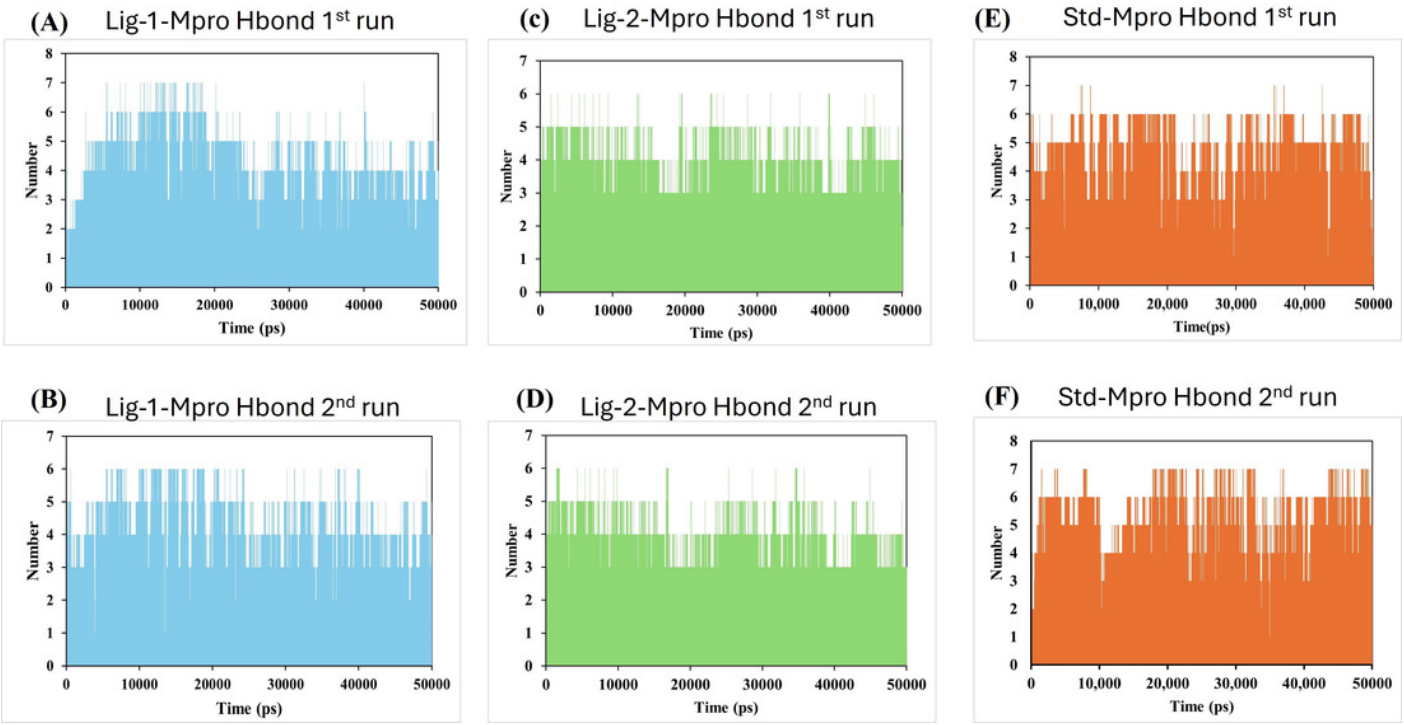

Figure 6

Figure 6. The hydrogen bond distance plot of compound Pentoxifylline with Mpro protein.

The plot indicates changes in the distance between key binding-site amino acids and the ligands over time during each MD simulation.

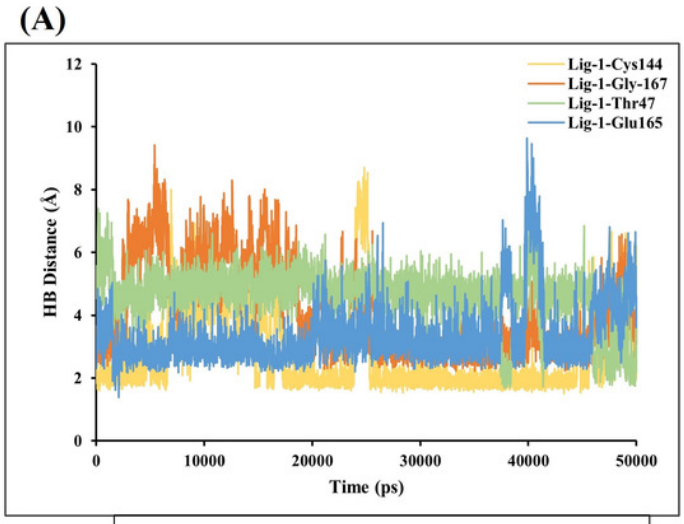

Lig-1-Mpro Hbond distance 1st run

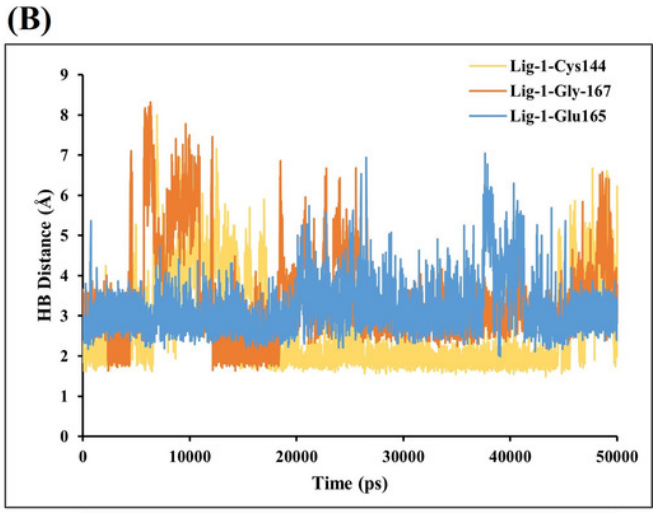

Lig-1-Mpro Hbond distance 2nd run

Figure 7

Figure 7. The hydrogen bond distance plot of compound Methotrexate with Mpro protein.

The plot indicates changes in the distance between key binding-site amino acids and the ligands over time during each MD simulation.

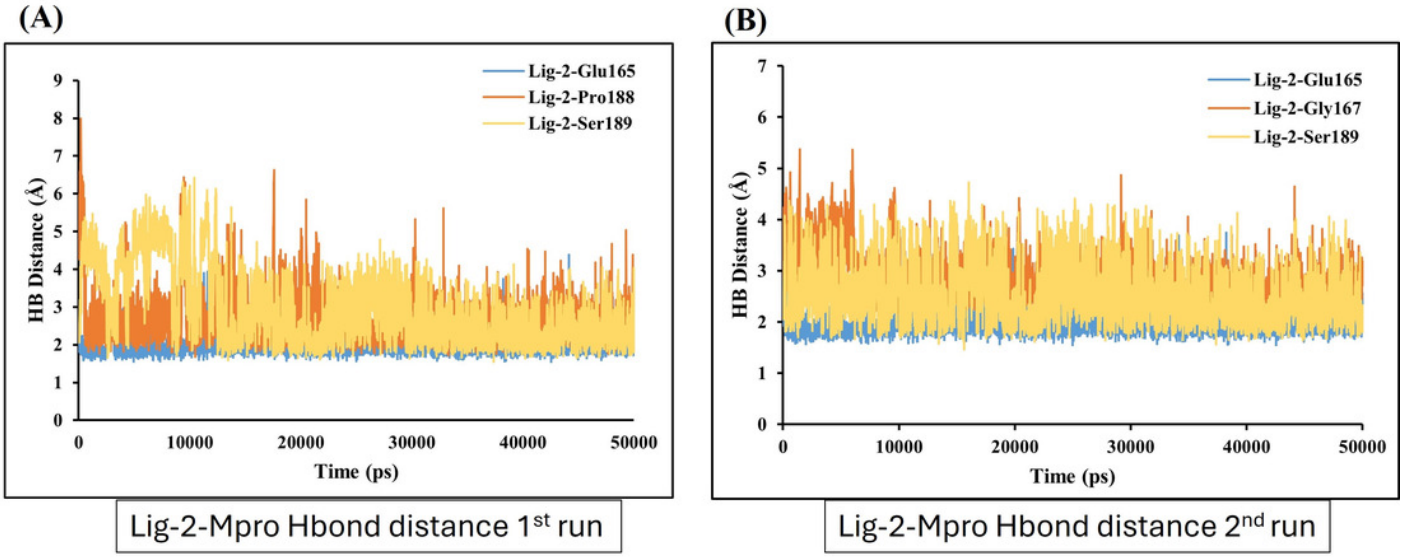

Lig-2-Mpro Hbond distance 1st run

Lig-2-Mpro Hbond distance 2nd run

Figure 8

Figure 8. The hydrogen bond distance plot of compound Sofosbuvir with Mpro protein.

The plot indicates changes in the distance between key binding-site amino acids and the ligands over time during each MD simulation.

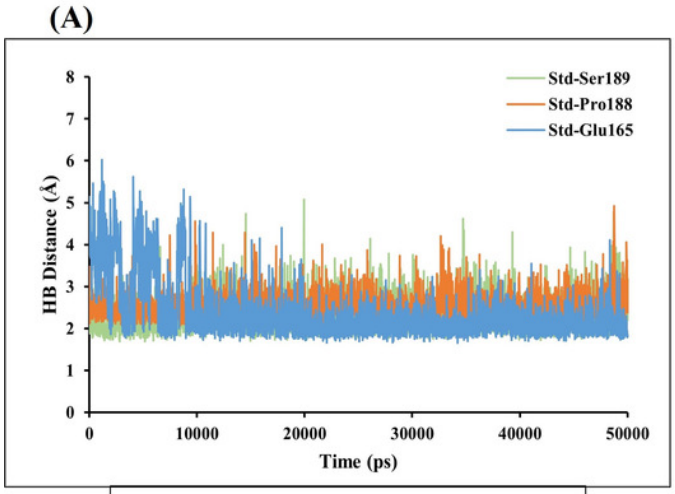

Std-Mpro Hbond distance 1st run

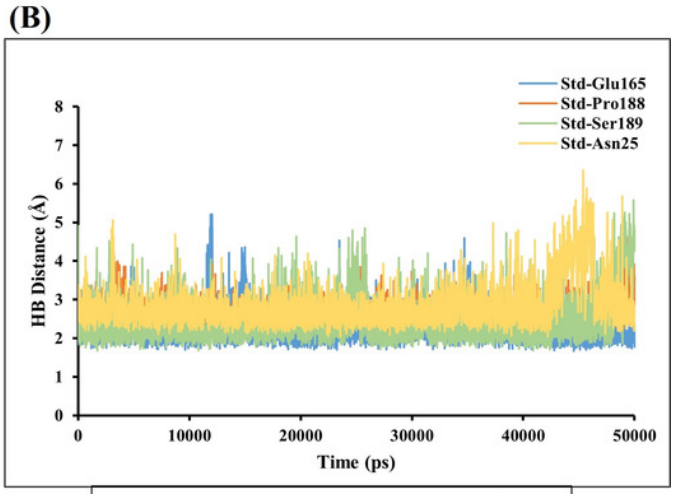

Std-Mpro Hbond distance 2nd run